1. Zulkifly AZIZ[1], 2. Mohd Mawardi SAARI[1,2,*], 3. Mohd Aufa Hadi Putera ZAINI[1], 4. Nurul A'in NADZRI[1], 5. Sim Yee CHIN[1,3]

Faculty of Electrical and Electronics Engineering Technology, Universiti Malaysia Pahang (1), Center for Advanced Industrial Technology, Universiti Malaysia Pahang (2), Center of Excellence for Advanced Research in Fluid Flow, Universiti Malaysia Pahang (3)
ORCID: 1. 0000-0003-0646-0473; 2. 0000-0002-3049-5548; 3. 0000-0001-6497-2739; 4. 0000-0003-3317-0236; 5. 0000-0002-9302-6917
*Corresponding author. E-mail address: mmawardi@ump.edu.my

doi:10.15199/48.2023.08.30

Improved wireless LED-based light emitters for photocatalytic oxidation in a slurry annular reactor

Abstract. *In this work, a custom-built ferrite rod was designed to replace the commercial ferrite drum core in a conventional wireless light emitter driven by wireless power transfer for photocatalytic oxidation of wastewater. Simultaneous improvement in coupling coefficient and quality factor was achieved, allowing maximum energy transfer. A coupling coefficient of 0.024 was achieved at the center of the field coil at zero angular misalignment for a coil quality factor of 74 measured at the switching frequency of 185 kHz. In addition, the emitter irradiation intensity could be regulated from 80 – 380 W/m^2, a useful feature in the situation where high intensity promotes the recombination of electrons and holes.*

Streszczenie. *W tej pracy zaprojektowano niestandardowy pręt ferrytowy, który ma zastąpić komercyjny rdzeń bębna ferrytowego w konwencjonalnym bezprzewodowym emiterze światła napędzanym bezprzewodowym transferem energii do fotokatalitycznego utleniania ścieków.Osiągnięto jednoczesną poprawę współczynnika sprzężenia i współczynnika jakości, umożliwiając uzyskanie maksymalnej energii Współczynnik sprzężenia 0,024 został osiągnięty w środku cewki polowej przy zerowej niewspółosiowości kątowej dla współczynnika jakości cewki 74 mierzonego przy częstotliwości przełączania 185 kHz.W/m2, użyteczna cecha w sytuacji, gdy wysokie natężenie sprzyja rekombinacja elektronów i dziur. (**Udoskonalone bezprzewodowe emitery światła oparte na diodach LED do fotokatalitycznego utleniania w zawiesinowym pierścieniowym reaktorze**)*

Keywords: photoreforming, photocatalyst, wireless coupler, slurry annular reactor.
Słowa kluczowe: fotoreformowanie, fotokatalizator, łącznik bezprzewodowy, zawiesinowy reaktor pierścieniowy.

Introduction

A century-old idea of wireless electricity is recently gathering momentum among the scientific and industrial community. After two decades after its inception by a group of MIT engineers, the world has witnessed a surge in the applications of near-field wireless power transfer (WPT) applications from consumer electronics such as inductive heating [1] and portable charging [2] to charging an electric vehicle [3] and implantable medical devices [4]. Photocatalytic oxidation of organic pollutants under ultraviolet (UV) or visible light irradiation is another field that could potentially benefit from near-field WPT.

Briefly, photocatalytic oxidation is a process energized by absorbing visible [5] or ultraviolet (UV) [6] energy radiation which triggers the separation of electrons and holes on photoactive sites. The liberated charge carriers then mediate the chemical transformation of organic pollutants in the presence of strong hydroxyl radicals [7].

Hayashi et al. initially proposed the idea of dispersing multiple miniature light sources inside a photocatalytic reactor by ultrasonic resonance and piezoelectric effect [8]. The proposed strategy achieved an 18 % increase in reaction rate compared to the internal and external illumination strategies employed in conventional photocatalytic reactors. The electro-sonification, however, required high power to operate. Kuipers et al. proposed to illuminate the interior of a photocatalytic slurry reactor using multiple ultraviolet light-emitting diodes (UV-LEDs) powered by WPT [9]. The goal was to increase the photon transfer efficiency by simultaneously increasing the number of light sources and distributing them throughout the reaction medium instead of having a single and static light source situated in the middle of the reactor [10] or mounted externally [11] as in the conventional system. Heining et al. applied similar illumination techniques to increase the culture volume of photosynthetic active microorganisms inside a cylindrical photobioreactor [12]. To eliminate the separation and filtration stage of the suspended photoactive materials from the treated solution in postprocessing, Burek et al. coated their light-emitting spherical balls with a photoactive catalytic layer [13]. To protect the spherical enclosure of the light emitter from interacting with the photoactive material, a protective layer of silicon dioxide (SiO_2) was required. In addition, significant loss of photocatalytic layer due to mechanical abrasion was also reported. In [14], the same illumination strategy was adopted for a pilot scale photobioreactor having a volume of 24.7 L and populated with 3000 wireless light emitters (WLEs). The author also disputed the series resonance topology implemented in [15] and showed that the topology did not work when it was simulated. The author argued that the proposed series resonance topology had failed because the resistance of the LED became high when the LED was reverse-biased. A better explanation was given by Schuylenbergh, who postulated that a parallel resonance secondary is associated with a voltage output for a large AC load, while a series resonant secondary with a current output is only matched to small AC load [16]. From literature search, it can be concluded that a series resonance secondary is suitable for a small AC load of less than 50 Ω [7, 17, 18] while the parallel resonance secondary is suitable for large AC load [7]. Therefore, a parallel resonant secondary is suitable to drive an LEDs with a typical AC load of ~200 Ω.

Experimental

The induced voltage V_{emf} in an inductive coil is given by [19, 20]:

$$V_{emf} = -N\frac{d\varphi}{dt} = -N\frac{d}{dt}\left(A \cdot B\cos\omega t\right) \quad (1)$$

where: N – number of turns, φ – flux, A – is the loop area perpendicularly interlinked by the magnetic field density B. Noting that $B = \mu H$, thus the field density can be proportionately scaled up in the presence of high permeability material so that a higher induced voltage can be obtained with a high magnetic flux φ interlinked to the coil [21]. Based on this reasoning, a ferrite core was implemented for the receiver.

The proposed experimental setup is shown in Fig.1. The discussion on the modified Helmholtz field coils has already been detailed elsewhere [22]. The field coils surrounded a 10.6 L acrylic cylinder filled with water to mimic an actual photocatalytic reactor environment. The receiver consisted of a parallel LC resonant circuit connected to LED loads. The LED used was a 5050 white LED from Solleds Inc. with peak emission at 425 nm and maximum power dissipation of 300 mW. The type of ferrite core used was 3C90, Ferroxcube with reported initial permeability of 2300 that is stable up to 1 MHz without significant core loss. In addition, a comparison against commercial surface mount device (SMD) power inductors from Sumida Inc., having roughly a similar footprint, was also carried out (drum dimensions summarized in Table 1) to gauge the effectiveness of the proposed design.

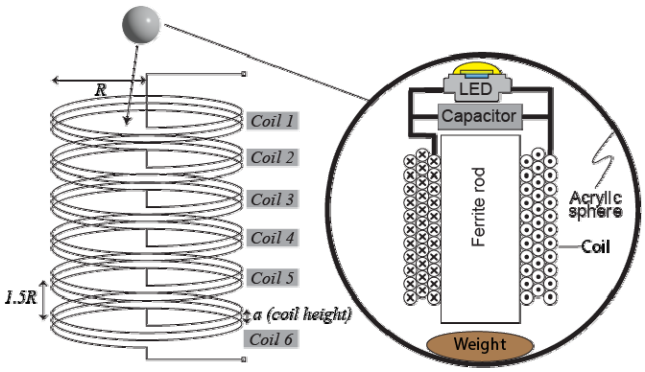

Fig. 1. Simplified schematic of the proposed experimental setup showing the modified Helmholtz field coils and the miniature light-emitting ball as the receiver.

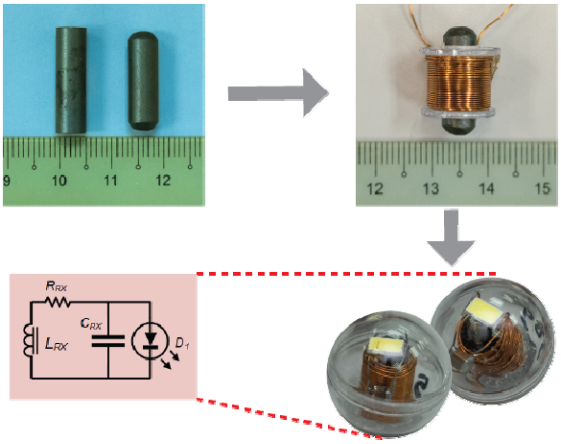

Fig. 2. Fabrication stages of the light-emitting ball.

Table 1. The parameters of the receiver

	Custom-built	Solleds CD105
Ferrite rod/drum dimension	15 (H) x 5 (D) mm	10.4 (L) x 9.4 (W) x 5.8 (H) mm
Coil dimension	14 x 5 mm	NA
Number of turns	100	112
Wire size	0.314 mm	0.1 mm
Weight	4.25-4.28 g	4.25-4.28 g
Inductance (μH)	315	475.2
Series resistance (Ω)	0.76	1.09
Quality factor, Q (185 kHz)	74	55

The receiving coil circuitry was sealed inside a watertight acrylic ball, as illustrated in Fig.2. To promote buoyancy while maintaining vertical alignment inside the magnetic field, the density of the light emitter was carefully calibrated by adding weight to its base so the receiver would stay upright when in motion inside the field coil. The receiver's specifications are summarized in Table 1.

The plot of intensity versus dissipated power for the LED was obtained through a calibration procedure, as illustrated in the schematics of Fig. 3.

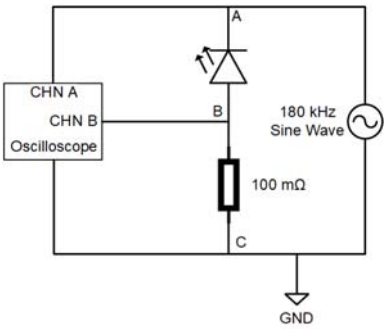

Fig. 3. Electrical schematic used to obtain the LED intensity versus power dissipated relationship.

The mutual inductance of the wireless coupler was obtained using an LCR meter, as illustrated in Fig. 4.

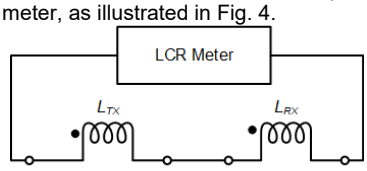

$$L_{total} = L_1 + L_2 + 2M$$

Fig. 4. The cumulative series connection used for the mutual inductance measurement.

Results and Discussion

Impedance Characteristics of the Receiving Coil

The peak observed in the impedance plot of Fig. 5 indicated that the receiving coil self-resonated at a much higher frequency of 1.9 MHz than the designed operating frequency of 185 kHz used in this study. At the designed switching frequency, the coil exhibited an equivalent series resistance (ESR) of 6.1 Ω. The coil Q factor peaked at around 65 kHz, and descended to about 50 at the designed operating frequency. These coil characteristics were measured for the coil with the ferrite rod core but without the resonance capacitor. It is worth noting that resonating would only shift the Q factor value to the desired operating frequency without affecting the value as could be seen in the following section.

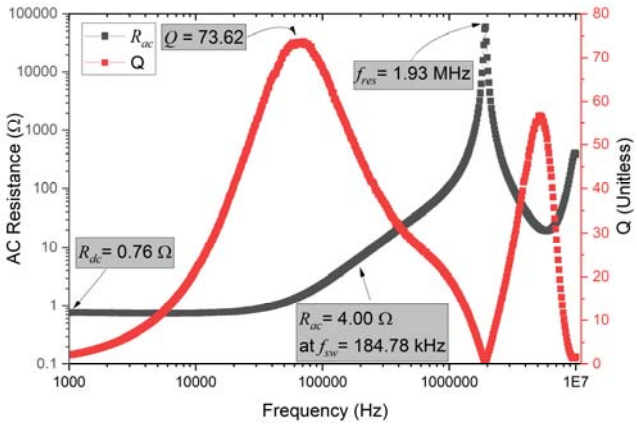

Fig. 5. The AC resistance plot of the receiving coil measured as a function of frequency showing the series resistance, ESR at the switching frequency and the self-resonant peak.

Power Requirements of LED

The relationship between input power and intensity of LED was plotted in Fig. 6. From the plot, it can be inferred that the relationship between the LED input power and intensity of irradiation was almost linear in the range of 50-400 W/m^2. As such the LED power requirement could be interpolated from the plot for a known value of irradiation intensity. The energy dissipated in each LED could be interpolated to obtain an estimate of the total dissipated energy in the multiple devices' environment.

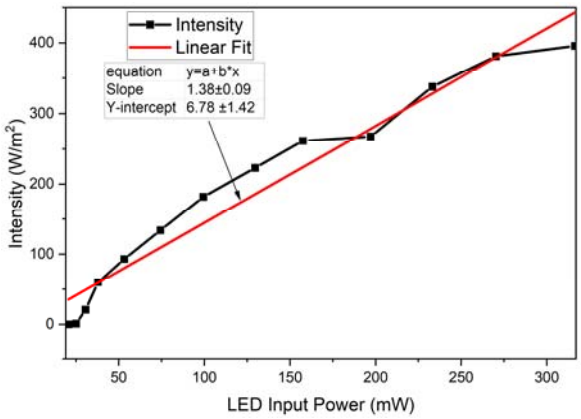

Fig. 6. Intensity as a function of input power.

Quality Factor

The quality factor Q of the receiving coil was plotted as a function of the number of turns, as shown in Fig. 7(a). The value of Q increased linearly with the number of turns up until 50 turns, beyond which the Q factor began a small and gradual downward trend up to 100 turns. The trend became more prominent as the number of turns was increased beyond 100 turns. Hence, a decent Q factor value for the receiver could still be obtained for coil windings between 50 to 100 turns.

The point where Q is at its maximum is given by the point of intersection in Fig. 7(b). The optimum number of turns determined from the following plot was 50 turns, and it could be said that Q reached saturation after 50 turns. For the custom-built receiver inductor, the number of turns was decided to be 100 for a fair comparison to the commercial SMD ferrite drum inductors and availability of resonant capacitance values. The fabricated 100-turn inductor resulted in $Q = 74$.

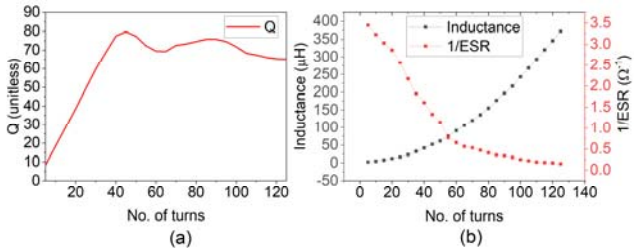

Fig. 7. The plot of (a) the measured quality factor of the receiving coil and (b) inductance with 1/ESR as a function of the number of turns.

The Q factor of several receivers built using the commercial SMD ferrite drum power inductors was plotted in the frequency range of interest from 100-200 kHz for comparison, as shown in Fig. 8. The plot showed the highest Q factor was obtained for the CD105 470 μH SMD type inductor, while the proposed custom-built receiver showing a slightly lower value without fluctuations and was stable from 100-200 kHz compared to other commercial SMD ferrite receivers. Despite the highest Q factor, the Solleds SMD type inductor also exhibited a slightly higher AC resistance (R_{ac}) value, in addition to increased fluctuations, as evident from the plot shown in Fig. 9. The higher R_{ac} value would incur more loss and higher voltage drop with less voltage delivered to the load. The rest of the SMD inductors either exhibited lower Q factor values or high R_{ac} value. Both conditions were not favored for efficient power transfer.

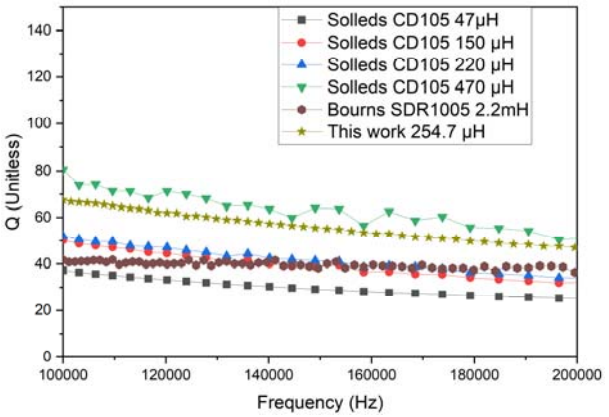

Fig. 8. Comparison of measured Q factors between custom-made and SMD-based receivers.

Since power transfer in a wireless coupler is governed by the product of Q and the coupling coefficient k, it can be inferred that the custom-made receiver would induce the highest voltage and produce the highest illumination intensity.

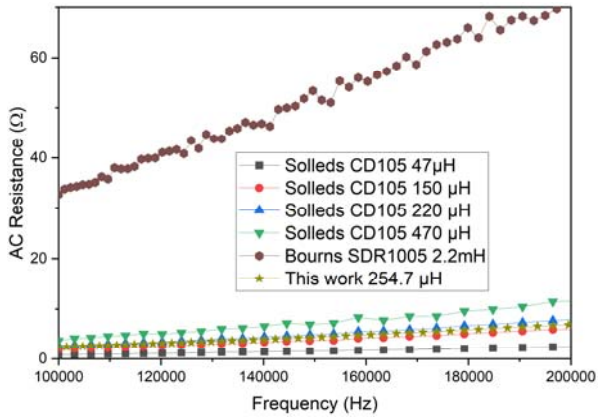

Fig. 9. The measured AC resistance

Mutual Inductance and Coupling Coefficient

It must be pointed here that the three SMD inductors from Solleds namely the CD105 with inductance values of 47, 150 and 220 μH respectively were of little interest here because they emit less than 60 W/m^2 when tested in the lab, hence they were excluded from this investigation. Table 2 compares the mutual inductance and the coupling coefficient values measured for the customized receiver against two other receivers types fabricated using commercial SMD inductors. While these receivers had different inductor footprints, the dimension of their drum sizes were roughly similar; hence their comparisons were justified. The highest k value of 0.024 obtained for the custom-built receiver would ensure that the LED would be brightly lit due to the highest energy transfer across the wireless coupler. Besides, the small mutual inductance value measured for the CD105 inductor type suggested weak magnetic coupling, an indication of poor quality in the used ferrite material. In addition, increased core windings would raise the inductance value considerably without

significant increase in the mutual inductance or the k coefficient as evident from the SDR1005 inductor type.

Table 2. Comparison between the mutual inductance and coupling coefficient values measured for three receiver types

	Custom-built	Solleds CD105	Bourns SDR1005
Mutual inductance at zero angular, vertical, and lateral displacement (μH)	12.55	3.35	12.95
No. of turn	100	112	250
Coupling coefficient, k	0.024	0.005	0.0091
Dimension of ferrite drum	14 (H) x 5 (D) mm	10.4 (L) x 9.4 (W) x 5.8 (H) mm	12.7 (L) x 7.6 (W) x mm
Inductance (μH)	315	475.2	2200
R_{AC} at 185 kHz (Ω)	4	5.5	68

Emitter's Intensity

The plot of the emitter's intensity as a function of the inverter's input voltage was plotted in Fig. 10. The plot demonstrated the regulation of intensity from 80 - 380 W/m^2 when the DC supply voltage to the inverter was varied between 9 - 18 V. This feature would be highly beneficial in situations where high irradiation intensity had lowered the reaction rate due to increased recombination of electron and holes. The power dissipated by the LED varied between 1 – 4.5 W for different intensity levels.

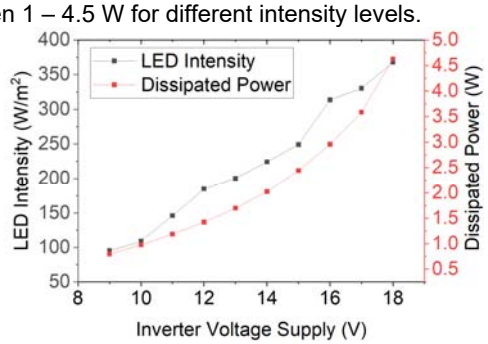

Fig. 10. The measured radiation intensity as a function of inverter input voltage.

Efficiency measurements

The efficiency of the proposed system was plotted as a function of inverter input voltage in Fig. 11. It can be inferred from the plot that the efficiency of the wireless coupler decreased with increasing supply voltage. This was due to junction heating in the LED which increased with increasing intensity. Initially, the effect was subtle for a single LED device but became more prominent when the receiving device was increased to six. The plot also revealed that the efficiency of the wireless coupler system was incremental, meaning the value would add up with an increasing number of LED devices inside the field coil. It was worth noting that the ferrite core used in the receiver would eventually alter the permeability of the transmitting medium. Thus, it can be inferred that the system efficiency value would follow an incremental fashion until the number of receiving devices began to significantly change the permeability of the reactor volume, thereby shifting the system's resonance frequency. At this point, the power transfer efficiency of the wireless coupler would begin to degrade.

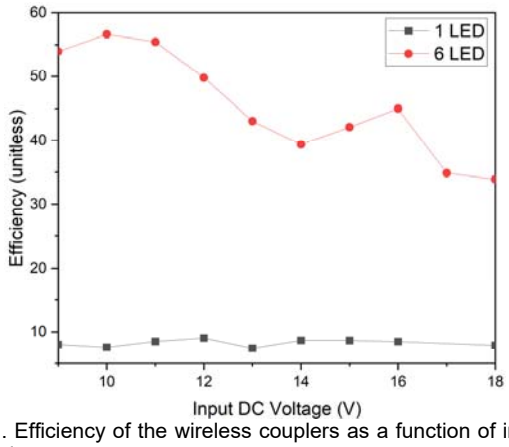

Fig. 11. Efficiency of the wireless couplers as a function of inverter input voltage.

Conclusions

A custom-built ferrite core was fabricated for a spherical LED-based light emitter to enhance the k coefficient to 0.024 and the Q factor to 74 simultaneously. Since the product of kQ determines the energy transfer across a wireless coupler, enhanced power transfer and extremely bright LED were obtained. The proposed wireless light emitter (WLE) could be used as a mobile light emitter to enhance the photon transfer efficiency in the photocatalytic oxidation of petrochemical wastewater.

***Acknowledgments**: The work was supported by the Ministry of Higher Education of Malaysia under the Trans-Disciplinary Research Grant Scheme TRGS/1/2018/UMP/02/2/1 (university reference RDU191802-1) and the Research Management Center of Universiti Malaysia Pahang under the grant number PGRS200337.*

***Author:** Zulkifly Aziz, E-mail: pek19002@student.ump.edu.my; assoc. prof. dr. Mohd Mawardi Saari (corresponding author), E-mail: mmawardi@ump.edu.my; Mohd Aufa Hadi Putera Zaini, E-mail: pek21001@student.ump.edu.my; Nurul A'in Nadzri, E-mail: pek19004@student.ump.edu.my, Universiti Malaysia Pahang, Faculty of Electrical and Electronics Engineering Technology, 26600 Pekan, Pahang Malaysia; assoc prof dr. Sim Yee Chin, Center of Excellence for Advanced Research in Fluid Flow, Universiti Malaysia Pahang, 26300 Gambang, Kuantan, Pahang, Malaysia, E-mail: chin@ump.edu.my.*

REFERENCES

[1] E. Plumed, I. Lope, J. Acero, and J. M. Burdío, Domestic Induction Heating System With Standard Primary Inductor for Reduced-Size and High Distance Cookware, IEEE Transactions on Industry Applications, vol. 58, no. 6, pp. 7562-7571, 2022, doi: 10.1109/TIA.2022.3193107.

[2] M. B. Lillholm, Y. Dou, X. Chen, and Z. Zhang, Analysis and Design of 10-MHz Capacitive Power Transfer With Multiple Independent Outputs for Low-Power Portable Devices, IEEE Journal of Emerging and Selected Topics in Power Electronics, vol. 10, no. 1, pp. 149-159, 2022, doi: 10.1109/JESTPE.2020.3035493.

[3] Y. Zhang, Z. Shen, W. Pan, H. Wang, Y. Wu, and X. Mao, Constant Current and Constant Voltage Charging of Wireless Power Transfer System Based on Three-Coil Structure, IEEE Transactions on Industrial Electronics, vol. 70, no. 1, pp. 1066-1070, 2023, doi: 10.1109/tie.2022.3150112.

[4] Z. Ye, M. Yang, and P. Y. Chen, Multi-Band Parity-Time-Symmetric Wireless Power Transfer Systems for ISM-Band Bio-Implantable Applications, IEEE Journal of Electromagnetics, RF and Microwaves in Medicine and Biology, vol. 6, no. 2, pp. 196-203, 2022, doi: 10.1109/JERM.2021.3120621.

[5] P. Manojkumar, E. Lokeshkumar, C. Premchand, A. Saikiran, L. Rama Krishna, and N. Rameshbabu, Facile preparation of immobilised visible light active W–TiO2/rGO composite photocatalyst by plasma electrolytic oxidation process, Physica B: Condensed Matter, vol. 631, 2022, doi: 10.1016/j.physb.2022.413680.
[6] N. Premalatha, P. Rajalakshmi, and L. R. Miranda, Photocatalytic degradation of Rhodamine B over TiO2/g-C3N4 and immobilized TiO2/g-C3N4 on stainless steel wire gauze under UV and visible light: A detailed kinetic analysis and mechanism of degradation, Reaction Kinetics, Mechanisms and Catalysis, vol. 135, no. 2, pp. 1031-1046, 2022, doi: 10.1007/s11144-022-02154-5.
[7] C. Rong, B. Zhang, Z. Wei, L. Wu, and X. Shu, A Wireless Power Transfer System for Spinal Cord Stimulation Based on Generalized Parity-Time Symmetry Condition, IEEE Transactions on Industry Applications, Article 2021, doi: 10.1109/TIA.2021.3090751.
[8] N. Hayashi, R. Yasutomi, and E. Kasai, Development of dispersed-type sonophotocatalytic process using piezoelectric effect caused by ultrasonic resonance, Ultrason Sonochem, vol. 17, no. 5, pp. 884-91, Jun 2010, doi: 10.1016/j.ultsonch.2009.12.017.
[9] J. Kuipers, H. Bruning, S. Bakker, and H. Rijnaarts, Near field resonant inductive coupling to power electronic devices dispersed in water, Sensors and Actuators A: Physical, vol. 178, pp. 217-222, 2012/05/01/ 2012, doi: 10.1016/j.sna.2012.01.008.
[10] S. Murgolo, S. Franz, H. Arab, M. Bestetti, E. Falletta, and G. Mascolo, Degradation of emerging organic pollutants in wastewater effluents by electrochemical photocatalysis on nanostructured TiO2 meshes, Water Res, vol. 164, p. 114920, Nov 1 2019, doi: 10.1016/j.watres.2019.114920.
[11] A. Chaudhuri, S. D. A. Zondag, J. H. A. Schuurmans, J. Van Der Schaaf, and T. Noël, Scale-Up of a Heterogeneous Photocatalytic Degradation Using a Photochemical Rotor-Stator Spinning Disk Reactor, Organic Process Research and Development, Review vol. 26, no. 4, pp. 1279-1288, 2022, doi: 10.1021/acs.oprd.2c00012.
[12] M. Heining, A. Sutor, S. C. Stute, C. P. Lindenberger, and R. Buchholz, Internal illumination of photobioreactors via wireless light emitters: a proof of concept, Journal of Applied Phycology, vol. 27, no. 1, pp. 59-66, 2015/02/01 2015, doi: 10.1007/s10811-014-0290-x.
[13] B. O. Burek, A. Sutor, D. W. Bahnemann, and J. Z. Bloh, Completely integrated wirelessly-powered photocatalyst-coated spheres as a novel means to perform heterogeneous photocatalytic reactions, Catal. Sci. Technol., vol. 7, no. 21, pp. 4977-4983, 2017, doi: 10.1039/c7cy01537b.
[14] A. Sutor, M. Heining, and R. Buchholz, A Class-E Amplifier for a Loosely Coupled Inductive Power Transfer System with Multiple Receivers, Energies, vol. 12, no. 6, p. 1165, 2019, doi: 10.3390/en12061165.
[15] J. Kuipers, H. Bruning, D. Yntema, and H. Rijnaarts, Wirelessly powered ultraviolet light emitting diodes for photocatalytic oxidation, Journal of Photochemistry and Photobiology A: Chemistry, Article vol. 299, pp. 25-30, 2015, doi: 10.1016/j.jphotochem.2014.10.017.
[16] K. v. Schuylenbergh and R. Puers. Inductive Powering, Basic Theory and Application to Biomedical Systems, p. 223, 2009.
[17] W. Zheng, F. Xie, W. Xiao, D. Qiu, and B. Zhang, Plane-Omnidirectional Wireless Power Transfer System Based on Vector-Controlled Flux Linkage, IEEE Access, Article vol. 9, pp. 105651-105666, 2021, Art no. 9497058, doi: 10.1109/ACCESS.2021.3100364.
[18] S. Sun, B. Zhang, C. Rong, X. Shu, and Z. Wei, A Multi-receiver Wireless Power Transfer System Using Self-oscillating Source Composed of ZVS Full-bridge Inverter, IEEE Transactions on Industrial Electronics, Article 2021, doi: 10.1109/TIE.2021.3066931.
[19] S. Tumanski, Induction coil sensors—a review, Measurement Science and Technology, vol. 18, no. 3, pp. R31-R46, 2007, doi: 10.1088/0957-0233/18/3/r01.
[20] S. TumaŃSki, Modern methods of electrical steel testing – a review, PrzeglĄd Elektrotechniczny, vol. 1, no. 3, pp. 164-169, 2021, doi: 10.15199/48.2021.03.31.
[21] S. Zurek, Systematic measurement errors of local B-coils due to holes, PrzeglĄd Elektrotechniczny, vol. 1, no. 3, pp. 8-14, 2018, doi: 10.15199/48.2018.03.02.
[22] Z. Aziz, M. M. Saari, C. S. Yee, M. A. H. P. Zaini, and N. A. i. Nadzri, Braiding Uniform Magnetic Field Inside a Cylindrical Reactor for Photocatalytic Reforming of Petrochemical Wastewater, pp. 1-8, 2020, doi: 10.1109/etcce51779.2020.9350888.